

Electronic Structure of gated graphene and graphene ribbons

J. Fernández-Rossier¹, J. J. Palacios¹, and L. Brey².

(1)Departamento de Física Aplicada, Universidad de Alicante, Spain

(2)Instituto de Ciencia de Materiales de Madrid, CSIC, Spain

(Dated: November 4, 2021)

We study the electronic structure of gated graphene sheets. We consider both infinite graphene and finite width ribbons. The effect of Coulomb interactions between the electrically injected carriers and the coupling to the external gate are computed self-consistently in the Hartree approximation. We compute the average density of extra carriers, n_{2D} , the number of occupied subbands and the density profiles as a function of the gate potential V_g . We discuss quantum corrections to the classical capacitance and we calculate the threshold V_g above which semiconducting armchair ribbons conduct. We find that the ideal conductance of perfectly transmitting wide ribbons is proportional to the square root of the gate voltage.

PACS numbers:

I. INTRODUCTION

One important ingredient of semiconductor microelectronics is the electrical tunability of the resistance through the field effect. The recent demonstration of field effect in graphene^{3,4,5} has opened a new research venue. Graphene is different from conventional semiconductors for a number of reasons. First, graphene is a truly two dimensional atomically thin layer of carbon atoms. Second, neutral graphene is a semimetal with zero density of states at the Fermi energy and zero gap, the two scales that shape the properties of metals and semiconductors. Third, the electronic structure close to the Fermi energy has a conical shape with perfect electron-hole symmetry and an internal valley symmetry, isomorphic to that of two dimensional massless Dirac fermions⁶. As a result, most of the standard lore on electronic and transport properties of low dimensional semiconductors needs to be revisited^{7,8,9,10}.

The presence of a band-gap in the electronic structure is crucial in the design of low dimensional structures and in the achievement of large on-off resistance ratios in field effect transistors (FETs). However, even at very low temperatures, two dimensional graphene shows a rather low resistance at the charge neutrality point^{1,3,4,10} at which the density of states at the Fermi energy is vanishingly small. A number of physical mechanisms that result in a gap in graphene based systems have been proposed: dimensional confinement into the so called graphene ribbons^{11,12,13,14,15}, interlayer coupling^{16,17} and spin polarization¹⁸. In this paper we focus on graphene ribbons, stripes of graphene with finite width W . Ideal graphene ribbons with edges along the crystallographic axis fall into two categories: zig-zag and armchair¹¹. Only the former can present a gap depending on their width W . Recent transport experiments with graphene ribbons¹⁹ confirm that ribbons with $W = 20nm$ present a thermally activated conductivity that indicates the presence of a gap. Most likely, imperfections on the edges of real ribbons make it hard to fabricate ribbons that are intrinsically metallic.

In this paper we explore the relation between gate voltage V_G and injected density in graphene-based field effect devices shown in figure 1. A graphene layer, of width W , lies on top of an insulating slab of thickness d which lies above the metallic gate. Application of a gate voltage V_G injects carriers in the graphene layer accompanied by a corresponding change in the metal. The main results of the paper are the following: (i) we show that V_G and the average two dimensional (2D) carrier density in the system, n_{2D} , satisfy the relation:

$$V_G = \frac{1}{C_{el}} en_{2D} + V_Q(n_{2D}) \quad (1)$$

where the first term arises from the classical electrostatic interaction and the second term, $V_Q(n_{2D})$, arises from quantum mechanical effects associated to the band structure of graphene. The classical contribution is dominant but it depends only on the geometry of the system. Although smaller, the second term contains information specific to the electronic structure of the system²⁰. (ii) we find that in 2D graphene the quantum contribution scales like $V_Q \propto \sqrt{n_{2D}}$, and from its measurement it would be simple to extract the linear slope of the graphene bands. (iii) in the case of ribbons we calculate the $V_G(n_{2D})$ curves for different widths W and we find the threshold gate above which semiconducting ribbons become metallic. (iv) We argue that the ideal conductance, G , in wide ribbons scales as $G = \sqrt{V_G}$.

The rest of this manuscript is organized as follows. In section II we describe the Hartree formalism that we use to calculate the electronic structure of gated graphene devices as well as the link between gate voltage and chemical potential. In section III we present the simple analytical solution of the self-consistent Hartree equation for planar graphene ($W = \infty$). We obtain an expression for the quantum capacitance of graphene and discuss the experimental implications. In section IV we present the numerical solution of the self-consistent Hartree equation for finite width armchair ribbons, both semiconducting and metallic, and we obtain n_{2D} and the conductance G as a function of W , and V_G . In section V we discuss the implications and present our conclusions.

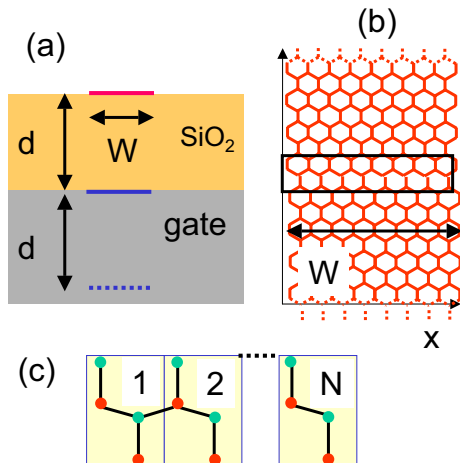


FIG. 1: (Color online). (a) Graphene based FET device: lateral view. A graphene ribbon of width W is separated from the metallic gate by an insulating slab of thickness d . The real charges of the metal are accumulated in the metal-insulator interface underneath the ribbon. Image charges lie further down the surface, at a distance $2d$ from the graphene. (b) Top view of an armchair graphene ribbon. The system is infinite along the vertical direction (y axis). (c) Detail of the super-unit cell defining the periodic one dimensional armchair ribbon.

II. THEORETICAL FRAMEWORK

A. Hamiltonian

We write the Hamiltonian for electrons in graphene as the sum of two parts: $H_0 + U$. The first term describes the electronic structure of neutral graphene. We approximate H_0 by the standard one-orbital tight-binding approximation for both the 2D graphene layer²¹ and graphene ribbons^{11,14,23}. The model is completely defined by the positions of the atoms, the first-neighbours hopping, $t = -2.5eV$, the lattice constant $a = 2.42\text{\AA}$, and the average density. The lattice of two dimensional graphene is characterized by a crystal structure defined by the two unit vectors $\vec{a}_{\pm} = \frac{a}{2}(\sqrt{3}, \pm 1)$ with a two atom basis. We assume that the graphene atoms lie in the $z = 0$ plane. In the case of neutral graphene, the average density is one electron per orbital that corresponds to a Fermi energy $E_F = 0$, since we take the on-site energy level equal to zero. The armchair ribbons considered in this paper are generated by one dimensional repetition of the super-cell of fig. 1b, along the y axis, with periodicity $\sqrt{3}a$. The supercell itself is constructed as the repetition of along the direction $(1, 0)$ of a block with 4 atoms (figure 1c). If the supercell has N blocks, the width of the ribbon is given by $W = Na$ and the number of atoms in the unit cell as $4N$. As a rule of thumb, it is useful to

write $W \simeq (N/4)nm$.

The second term U describes the Coulomb interaction between the extra charges in the system:

$$U = e \int \delta\hat{n}(\vec{r})\phi_{ext}(\vec{r})d\vec{r} + \frac{e^2}{2\epsilon} \int \frac{\delta\hat{n}(\vec{r})\delta\hat{n}(\vec{r}')}{|\vec{r}-\vec{r}'|}d\vec{r}d\vec{r}' \quad (2)$$

where $\delta\hat{n}(\vec{r})$ is the operator describing the departure of the local the electronic density from charge neutrality:

$$\delta\hat{n}(r) \simeq \sum_{I,\sigma} |\phi_I(r)|^2 (c_{I,\sigma}^\dagger c_{I,\sigma} - n_0) . \quad (3)$$

Here the sum runs over all the atoms in the lattice and $\phi_I(r)$ denotes the π_z atomic orbital centered around the atom I and $c_{I,\sigma}^\dagger$ is the second quantization operator that creates one electron with spin σ in the orbital $\phi_I(r)$, localized around atom I . In Eq.3 $n_0 = 1/2$ is the number of electrons per site and per spin in neutral graphene.

The electrostatic potential created by the extra charges in the metallic gate is denoted by $\phi_{ext}(\vec{r})$. Considered as a whole, the graphene and the metal layer form a neutral system. Therefore, the extra carriers in one side are missing in the other. Since the charges in the metallic gate move as to cancel the electric field inside the metal, they depend on the density distribution in the graphene electrode, which in turn depends on $\phi_{ext}(\vec{r})$. This self-consistent problem is solved using the image method: for a given charge density profile in the graphene, $e\langle\delta\hat{n}(\vec{r})\rangle$ the potential created by the corresponding extra charges in the metal is given by a distribution of fictitious image charges inside the metal: $-e\delta n_{im}(\vec{r}) = -e\delta n(\vec{r}-2\vec{d})$ with $\vec{d} = (0, 0, d)$.

$$V_{ext}(\vec{r}) = -\frac{e}{\epsilon} \int \frac{\langle\delta\hat{n}(\vec{r}')\rangle}{|\vec{r}-\vec{r}'+2\vec{d}|}d\vec{r}' . \quad (4)$$

With this method the potential evaluated at the metal gate ($z = 0$) is exactly zero. Therefore, the potential difference between the metal-insulator interface and the graphene layer is the potential evaluated at the graphene layer.

B. Hartree approximation

The electronic repulsion is treated in the Hartree approximation. Therefore, the electrons feel the electrostatic potentials created by both the gate and themselves:

$$\hat{U} \simeq \hat{U}_{SC} = e \int \delta\hat{n}(\vec{r}) (V_{ext}(\vec{r}) + V_{SC}(\vec{r})) d\vec{r} \quad (5)$$

The argument of the integral, $V_T \equiv V_{ext} + V_{SC}$, can be written as

$$V_T(\vec{r}) = \frac{e}{\epsilon} \int \langle\delta n(\vec{r}')\rangle \mathcal{K}(|\vec{r}-\vec{r}'|, d) d\vec{r}' \quad (6)$$

where

$$\mathcal{K}(|\vec{r} - \vec{r}'|, d) = \frac{1}{|\vec{r} - \vec{r}'|} - \frac{1}{|\vec{r} - \vec{r}' + 2\vec{d}|} \quad (7)$$

In the Hartree approximation $H_0 + U_{SC}$ is a one-body Hamiltonian that can be represented in the basis of localized π_z atomic orbitals. The H_0 part yields the standard single orbital tight-binding Hamiltonian. In contrast, the U_{SC} introduces site-dependent shifts in the diagonal matrix elements:

$$U_I = eV_I = \frac{1}{\epsilon} \sum_J q_J v_{IJ} \quad (8)$$

where q_J is the average excess charge in site J and $v_{IJ} = \int d\vec{r} d\vec{r}' |\phi_I(\vec{r})|^2 |\phi_J(\vec{r}')|^2 \mathcal{K}(|\vec{r} - \vec{r}'|, d)$, is the potential created by an unit charge located at site J on site I . At this point we adopt an approximation which permits to evaluate v_{IJ} without a detailed model of $\phi_I(\vec{r})$. Since the atomic orbitals are highly localized, for $|R_I - R_J| > a$ we can approximate v_{IJ} by the first term in the multipolar expansion: $v_{IJ} \simeq \frac{1}{|\vec{R}_I - \vec{R}_J|} - \frac{1}{|\vec{R}_I - \vec{R}_J - 2\vec{d}|}$. We have verified that the potential in a given site is quite independent of the approximation adopted to evaluate the $I = J$ contribution, for which the monopolar approximation fails. Without sacrificing accuracy, we adopt the simplest strategy of removing that term from the sum.

The Schrödinger equation reads

$$(H_0 + U_{SC})|\alpha\rangle = \epsilon_\alpha|\alpha\rangle \quad (9)$$

where the eigenvectors $|\alpha\rangle$ are linear combinations of atomic orbitals: $|\alpha\rangle = \sum_I \mathcal{C}_{I,\alpha} |\phi_I, \sigma\rangle$, and the coefficients are independent of the spin because we only consider non-magnetic solutions. In turn, the distribution of excess charges depends on the eigenvalues and eigenvectors through the equation

$$q_J = e \left[\sum_{\alpha,\sigma} (|\mathcal{C}_{I,\alpha}|^2 f(\epsilon_\alpha)) - 1 \right] \quad (10)$$

where $f(\epsilon_\alpha)$ is the Fermi function.

Equations (8), (9) and (10) need to be solved iteratively. In each step of the iterative procedure we have an *input* distribution of extra charge, q_I which results in a potential (eq. (8)), which defines a Hamiltonian whose eigenstates (eq. (9)) result in an *output* distribution of extra charge (eq. (10)). The converged solution is such that the input and output distribution of charges are the same. We refer to that distribution and the corresponding Hamiltonian as the self-consistent solution.

C. Gate voltage, chemical potential and quantum capacitance

In real field effect devices, application of a gate voltage V_G results in a change of carrier density in the active

layer. In our theoretical framework, we define eV_G as the the chemical potential difference between the metallic backgate and the graphene ribbon, necessary to accommodate extra carriers (either holes or electrons) in graphene and remove them from the metallic backgate:

$$eV_G(n_{2D}) = \mu_{graphene} - \mu_{metal} \quad (11)$$

where n_{2D} is the average two-dimensional density of *extra* carriers. In general, there are two contributions to the dependence of the chemical potential on n_{2D} . One one side, the presence of the electrostatic potential created by extra carriers present both in graphene and the metallic backgate shifts and modifies the bands. We refer to the new bands as the Hartree bands. On the other, addition of new carriers involves an additional shift of the chemical potential with respect to the Hartree bands. Whereas the first contribution has a classical origin, the second is a consequence of the Pauli principle and we refer to it as quantum contribution to the capacitance. We neglect a third type of contribution, arising from the modification of the bands due to density dependent exchange and correlation contributions²⁰.

The extra carriers in the metallic gate are concentrated on the surface so that the *bulk* chemical potential and the *bulk* energy bands are shifted by the same amount: there is no quantum contribution to the capacitance coming from the bulk metal. Things are different in the graphene layer. In this case, it makes no sense to talk about bulk and surface as different objects. In graphene, the chemical potential has to shift relative to the modified bands in order to accommodate extra carriers, resulting in a non-zero quantum contribution to the capacitance. Without loss of generality we take the metallic side as the reference for the electrostatic contribution to the chemical potential. This permits to write

$$eV_G = \mu_{graphene}(n_{2D}) - \mu_{graphene}(0) \equiv \delta\mu \quad (12)$$

From an operational point of view, we consider the system to be at zero temperature, and we take the chemical potential of graphene at a given density as the lowest unoccupied eigenstate of the self-consistent Hamiltonian. Identical results are obtained from the equation

$$n_{2D} = \int_{-\infty}^{\mu} \rho_{SC}(E) dE \quad (13)$$

that relates the chemical potential, the extra density via the density of states of the self-consistent Hamiltonian, $\rho_{SC}(E)$.

III. CLASSICAL AND QUANTUM CAPACITANCE OF PLANAR GRAPHENE

In the case of 2D graphene all the atoms of the lattice are equivalent and therefore the extra charge q_I and the effective potential U_I are independent of the location. As

a matter of fact, for an average extra density n_{2D} , the electrostatic potential is $U_I = \frac{4\pi e^2}{\epsilon} n_{2D} d$. Therefore, the Hartree bands of charged graphene are equal to the bare bands plus a rigid shift:

$$E_\nu(\vec{k}) = \epsilon_\nu^0(\vec{k}) + \frac{4\pi e^2}{\epsilon} n_{2D} d \quad (14)$$

In figure 2 (left panels) we plot both the bare bands $\epsilon_\nu^0(\vec{k})$ and the Hartree bands $E_\nu(\vec{k})$ for $d = 300\text{nm}$ and a $n_{2D} = 10^{12}\text{cm}^{-2}$. We see that Hartree bands are shifted upwards. Accordingly, the shift in the chemical potential needed to accommodate this extra charge will have to account for the electrostatic shift of the bands. On top of that, the chemical potential needs to move away from the Dirac point, which is also shifted electrostatically. In order to calculate this second contribution, we restrict ourselves to the energy region around $E_F = 0$ in which the density of states is linear (linear bands in 2D). This is a very good approximation since we consider $n_{2D} \ll n^0 \simeq 3.9 \cdot 10^{15}\text{cm}^{-2}$, the equilibrium electronic density in graphene. Therefore we write the density of states of the self-consistent Hamiltonian:

$$\rho_{SC}(E) = \rho_0 \left(E - \frac{4\pi e^2}{\epsilon} n_{2D} d \right) \quad (15)$$

with: $\rho_0(E) = \frac{8}{3\pi t^2 a^2} |E|$

After some simple steps we write the equation relating the change in chemical potential $\delta\mu$

$$n_{2D} = \int_0^{\delta\mu} \rho_{SC}(E) dE \quad (16)$$

which yields

$$n_{2D} = \frac{8}{3\pi} \frac{1}{2t^2 a^2} \left| \delta\mu - \frac{4\pi e^2}{\epsilon} n_{2D} d \right|^2 \quad (17)$$

From here we obtain one of the important results of this work:

$$eV_G = \frac{4\pi e^2}{\epsilon} d n_{2D} + |t| \sqrt{\frac{6\pi n_{2D} a^2}{8}} \equiv \frac{e n_{2D}}{C_{el}} + eV_Q \quad (18)$$

Thus, we write the gate voltage as the sum of two terms. The first is the standard electrostatic contribution whereas the second is related to the density of states of graphene. We refer to the second, V_Q , as the quantum contribution to the gate voltage (or inverse capacitance). In most of devices so far^{1,3,4,10} $d \simeq 300\text{nm}$, which makes the electrostatic contribution much larger than the quantum contribution. In figure 2b we plot V_G vs n_{2D} , according to equation (18). In spite of the last term of eq. (18), the curve looks like a straight line. As in refs. (3,4) we have done a linear fit of fig. 2b obtaining $n_{2D} = \alpha V_G$ with $\alpha = 0.718 \cdot 10^{11} \text{V}^{-1} \text{cm}^{-2}$, in very good agreement with the experiments. In order to reduce the electrostatic contribution as much as possible, in figure 2c we consider

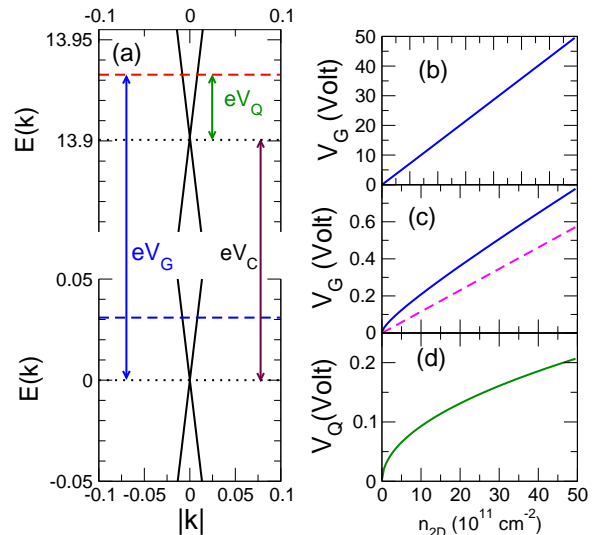


FIG. 2: (Color online). (a): Bare (below) and Hartree (above) bands, close to the Dirac point, of two dimensional graphene with $n_{2D} = 10^{12}\text{cm}^{-2}$. The vertical lines represent the chemical potential of the charged system, eV_G , which is the sum of two contributions, eV_C , the rigid shift of the bare bands to yield the Hartree bands, and eV_Q , the shift of the chemical potential with respect to the Hartree bands, the quantum contribution to the gate. Dotted horizontal lines represent the bare and charged Dirac points and dashed horizontal lines the bare and charged chemical potential. (b) $V_G = V_C + V_Q$ versus density for 2D graphene in a FET with $d = 300\text{nm}$ and $\epsilon = 3.9$. (c) $V_G = V_C + V_Q$ (solid line) and V_C (dashed line) versus density for 2D graphene in a FET with $d = 30\text{nm}$ and $\epsilon = 47$ (see for instance 22) (d) Quantum contribution to the gate, V_Q versus n_{2D} .

a thinner dielectric ($d = 30\text{nm}$) with a much larger dielectric constant $\epsilon = 47^{22}$. We see how in this case the gate voltage (solid line) is significantly different from the electrostatic contribution (dashed line). In figure 2d we plot the quantum contribution, which is independent of ϵ and d , alone. Although much smaller than the classical term, it can be larger than 0.2 Volt and it should be possible to measure it. Therefore, the independent measurement of n_{2D} , via classical Hall effect, and V_G could provide a direct measurement of the slope of the bands in the linear region if the experimental results are fitted using eq. (18).

IV. SELF-CONSISTENT ELECTRONIC STRUCTURE OF ARM-CHAIR RIBBONS

A. Bands and charge profiles

We now consider finite width armchair ribbons. They are different from two dimensional graphene both because their electronic structure and their electrical capacitance. Armchair ribbons are metallic (figure 3a,c) when the width of the sample has the form $W = (3M + 1)a_0$,

with M an integer, and insulating otherwise (figure 3b,d). In both case the electronic structure is different of the semimetallic behaviour of 2D graphene. On the other side, the presence of edges breaks translational invariance along the direction perpendicular to the ribbon axis. The edges provide a natural surface to accommodate the extra electrons. Therefore, the local potential and the extra charge profile are expected to vary as a function of the distance to the ribbon edge, keeping their translational invariance along the ribbon axis. This makes it harder to separate classical and quantum contributions to the capacitance in simple terms.

In figure 3 we show both the self-consistent (upper panels) and the neutral (lower panels) bands for electrically doped ribbons in two cases, semiconducting and a metallic ($N = 9$ and $N = 10$ respectively). Notice that charge neutral bands have electron-hole symmetry, like the semiconducting carbon nanotubes²⁴. In those figures we plot the self-consistent chemical potential in the upper panels and the naive Fermi energy obtained upon integration of the neutral density of states. As in the case of 2D graphene, the electrical injection of extra carrier results in a large shift of the bands, due to the electrostatic interactions. In contrast to the 2D case, the inhomogeneity of the electronic density and the electrostatic potential result in a moderate change of the the shape of the bands. Notice for instance that for the $N = 9$ ribbon the chemical potential intersects 2 self-consistent bands whereas the naive Fermi energy intersects 3 neutral bands.

As in the two dimensional case, the self-consistent chemical potential can be thought as the sum of a large electrostatic shift and a smaller quantum shift with re-

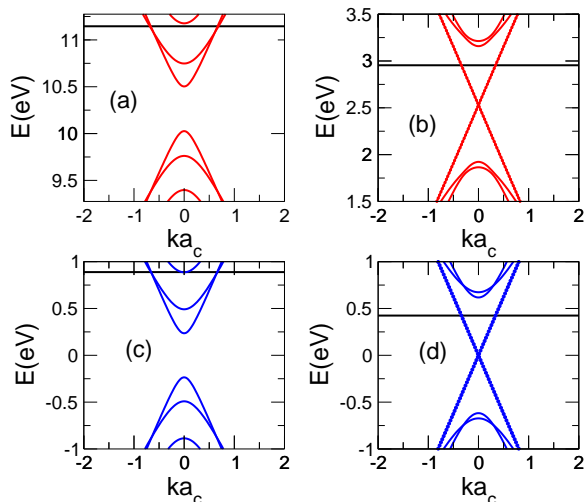


FIG. 3: (Color online). Energy bands for $N = 9$ (left panels) and $N = 10$ (right panels). The Hartree (bare) bands are shown above (below). The corresponding densities are $n_{2D} = 7.610^{12} \text{ cm}^{-2}$ ($N=9$) and $n_{2D} = 1.710^{12} \text{ cm}^{-2}$ ($N=10$). Notice that the neutral and Hartree bands are shifted with respect to each other. The horizontal lines indicates the Fermi energy.

commode the extra carriers. However, the electrostatic contribution to the gate depends not only on the average to density n_{2D} , like in the 2D case, but also on the detailed profile q_I . As a result, the separation of the chemical potential in two contributions, electrostatic and quantum mechanical, does not yield a simple procedure to

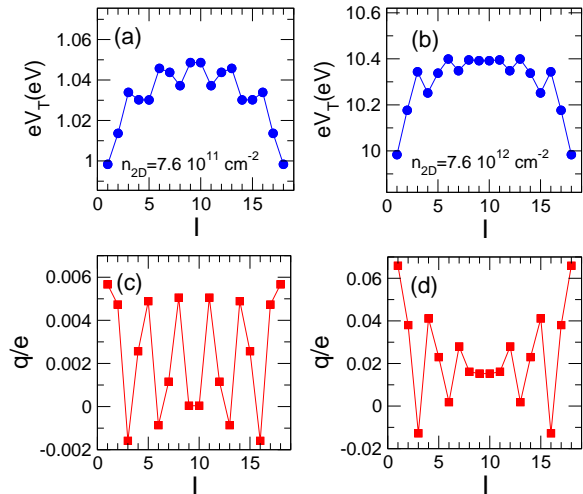


FIG. 4: (Color online). Potential ((a),(b)) and density ((c),(d)) profiles, as function of the position across the ribbons, for $N = 9$ ribbon with $n_{2D} = 7.6 \cdot 10^{11} \text{ cm}^{-2}$ (a,c) and $n_{2D} = 7.6 \cdot 10^{12} \text{ cm}^{-2}$ (b,d). The higher density results correspond to the bands shown in figure 3a.

In figure 4 we show the self-consistent density profile q_I and the self-consistent electric potential U_I for a semiconducting ribbon $N = 9$ with two different n_{2D} . We see how the density of carriers is larger in the edges than in the middle of the ribbon, as expected in a conducting system. As a result, the electrostatic potential has an inverted U shape. Superposed with these overall trends, both q_I and U_I feature oscillations, arising from quantum mechanical effects. Expectedly, the average U_I is much larger in the high density than in the low density. In the high density case it is apparent that the potential is flat in the inner part of the ribbon, very much like in a metal. Very similar trends are obtained for ribbons with different widths.

B. Density vs V_G

In figure 5a we plot the gate versus the average 2D extra density in graphene ribbons with for different widths N , indicated in the figure. This can be a valuable information to estimate the carrier density in gated ribbons since Hall measurements in narrow ribbons might be difficult to perform. The common feature in all the curves is the linear relation between V_G and n_{2D} that reflects the dominance of the classical electrostatic contribution

over quantum effects, exactly like in the 2D case. This is also apparent from figure 3, where the shift of the bands is much larger than the Fermi energy with respect to the bottom of the conduction bands. In addition, we see that some of the curves do not intersect at $V_G = 0$ for $n_{2D} = 0$ in the case of semiconducting ribbons. This is clearly the case of $N = 9$ and $N = 20$. In contrast, the curve $N = 10$ extrapolates to zero. We denote the threshold gate potential as V_{th} , and we notice that it corresponds to the change in chemical potential of the ribbon when a single electron is added. Since the chemical potential for a semiconductor system lies in the middle of the gap and the chemical potential when a single electron is added is the lowest energy state of the conduction band, we must have $eV_{th} = \frac{E_g}{2}$ where E_g is the gap of the semiconducting ribbon. We fit all the curves in figure 5a according to:

$$n_{2D}(N) = \alpha(N) (V_G - V_{th}(N)) \quad (19)$$

In figures 5b and 5c we plot α and V_{th} as a function of the ribbon width, N . The wider ribbon considered has $N = 60$ which corresponds to $W = 14.5\text{nm}$. In figure 5b we see how α rapidly decreases towards the 2D value $\alpha = \frac{e^2 d}{\epsilon} = 0.7 \cdot 10^{11} \text{cm}^{-2} \text{V}^{-1}$ as W increases. We have verified that α scales inversely proportional to the width N . Interestingly, $\alpha(N)$ approaches the two dimensional case very quick, even if $W \ll d$. The evolution of V_{th} as a function of N reflects two facts: on one side, 2 out of 3 ribbons are semiconducting. On the other, the gap decreases as W^{-1} . The evolution of the gap as a function of W in the one-orbital tight-binding calculation similar but not identical, to that obtained with density functional calculations¹⁸. Notice that ribbons of $W = 20nr$ ($N \simeq 80$) still present a gap¹⁹ and, according to figure 5b, their capacitance is almost that of two dimensional graphene.

C. Ideal Conductance vs V_G

We now study the number of occupied bands \mathcal{N} in a given ribbon as a function of V_G . This is related to the ideal conductance as a function of V_G through the Landauer formula for perfectly transmitting ribbons:

$$G = \frac{2e^2}{h} \mathcal{N} \quad (20)$$

This is equivalent to neglect the effect of disorder in the system. Therefore, the value of conductance so obtained can be considered an upper limit for the real conductance in the system²³. In an ideal armchair ribbon the number of channels \mathcal{N} increases in one by one as Fermi energy with respect to the Dirac point is increased. Our approach permits to obtain both \mathcal{N} and the quantum shift of the chemical potential as a function of the gate voltage and to plot \mathcal{N} as a function of V_G .

It must be stressed that in the 2D case this disorder free model⁸ accounts for the experimental results³. This

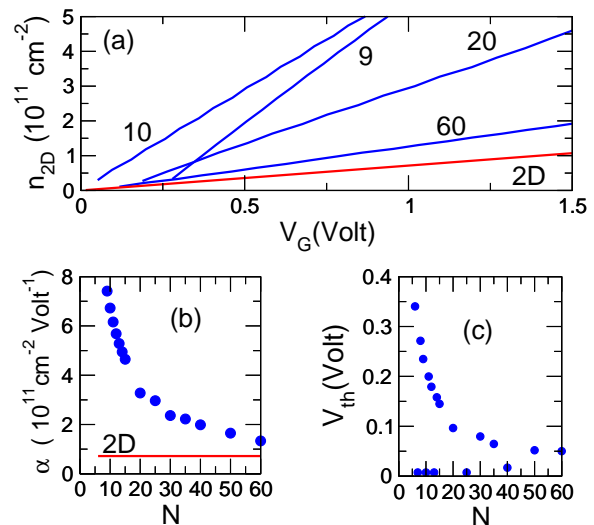


FIG. 5: (Color online). **a** Gate voltage versus average density for armchair ribbons of different widths. **b** Inverse capacitance, α , as a function of width (measured in terms of N). **c** Threshold voltage as a function of the ribbon width N .

might indicate that either disorder is not present in the samples or, more likely, because of the suppression of the backscattering it does not affect significantly the transport properties of graphene⁸. Transport on 2D graphene is being extensively studied by a number of groups. The effect of imperfections on the transmission of otherwise

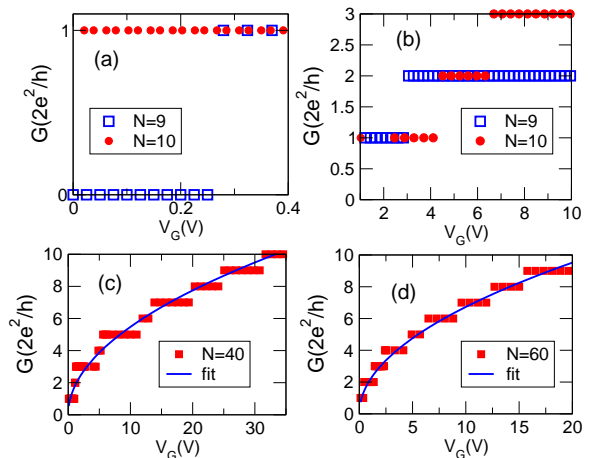


FIG. 6: (Color online). Conductance as a function of V_G for ribbons with $N = 9$ and $N = 10$ (a) and (b), $N = 40$ (c) and $N = 60$ (d) (see text)

In figure 6 we plot $G(V_G)$ for various ribbons. In figure 6a we plot the conductance $G(V_G)$ for two narrow ribbons ($N = 9$ and $N = 10$) in the small gate regime. It is apparent that the $N = 9$ ribbon only conducts above a threshold gate whereas the $N = 10$ ribbon is conducts even for $V_G = 0$. Therefore, semiconducting ribbons can

be electrically tuned from insulating to conducting behaviour with a gate voltage. This is also different from the case of 2D graphene which has a rather low resistance in the charge neutrality point. In figure 6b we show the conductance for the same ribbons at higher V_G . The different sizes of the plateaus for $N = 9$ and $N = 10$ reflect the different structure of the bands, as seen in figure 3. In figures 6c and 6d we show the conductance for wider ribbons ($N = 40$ and $N = 60$ respectively). Although the shape of the curves is superficially similar for all these ribbons, the V_G necessary to have a fixed number of bands at the Fermi energy is a decreasing function of W . This is a consequence of quantum confinement: the smaller the ribbon the larger the sub-band level spacing, $\Delta E_n = E_n(k=0) - E_{n-1}(k=0)$. A shift of the Fermi energy, relative to the self-consistent bands, by an amount ΔE_n , so that a new band is available for transport, implies also an electrostatic overhead, due to the change in density, which accounts for most of the eV_G , as we have discussed above.

In average, the steps in the stepwise curve $\mathcal{N}(V_G)$ increase size as V_G increases. This trend is more apparent in wider ribbons. In this sense it can be said that \mathcal{N} is sublinear in V_G . In the limit of very wide ribbons, for which the density of states is almost 2D, we can derive a qualitative relation between number of channels and V_G . Since the number bands per unit energy is roughly constant, we have that \mathcal{N} scales linearly with the Fermi energy with respect to the bottom of the bands, $\mathcal{N} \propto V_Q$. On the other side, we know that the density of carriers scales linearly with V_G (figs. 2 and 5) and, using the 2D density of states we know that density of carriers scales with $V_G \propto n \propto V_Q^2$. Therefore, we conclude

$$\mathcal{N} \propto \sqrt{V_G} \quad (21)$$

In figures 6c and 6d we have fitted the numerical data to the curve $G = aV_G^b$, where a and b are fitting parameters. We have obtained exponents $b = 0.45$ and $b = 0.47$ for $N = 40$ and $N = 60$ respectively, in agreement with the qualitative discussion above. In figure 6c and 6d we the solid line is the best fit to the equation $G = a\sqrt{V_G}$. Equation (21) is a re-statement of the relation between V_Q and n_{2D} of eq. (18). In both cases the exponent $1/2$ comes from the linear relation between energy and momentum of the two dimensional carriers on one side, and the quadratic relation between n_{2D} and Fermi momentum on the other. Therefore, eq. (18) and (21) are specific predictions related to the peculiar Dirac-like spectrum of electrons in graphene.

V. DISCUSSION AND CONCLUSIONS

In this work we study how the electronic structure and the density of carriers of graphene based field effect transistors evolve as a gate voltage V_G is applied. An impor-

tant notion is the identification of eV_G as the change in chemical potential in the graphene layer necessary to accommodate the density of extra carriers n_{2D} . The change in chemical potential is the sum of a electrostatic contribution, independent of the details of the electronic structure of graphene and a quantum contribution that depends on the details of the graphene band structure. In the case of 2D graphene, we have obtained a particularly simple equation (18) relating these quantities. We find that the quantum contribution is sufficiently small as to go unnoticed in the experiments done so far^{1,3,4}, but sufficiently big as to be measured. Even more important, we claim that an independent measurement of n_{2D} and V_G would provide a direct measurement of the slope of the linear energy bands, the so called graphene "speed of light".

We have considered idealized armchair ribbons which, at the charge neutrality point, can be either semiconducting or metallic. Application of a eV_G equal to half the band-gap turns semiconducting ribbons into conductors. This affords a on/off ratio much larger than that of 2D graphene. In the case of graphene ribbons the classical contribution to capacitance depends on the charge density profile q_I in the ribbon (fig. 3), which can not be measured easily, and we can not provide a simple experimental procedure to extract information about the electronic structure of the ribbons out of the $V_G(n_{2D})$ curves. We find that density of extra carriers is higher in the edges of the ribbons than in the middle.

Future work should address the issue of the stability of the results obtained in this paper with respect to disorder. In particular, we expect that disorder will turn metallic ribbons into semiconducting at $V_G = 0$. In figure 3 it is apparent that the metallic character of the ribbon with $N = 10$ comes from the states lying in a narrow window of width Δk_x around $k_x = 0$ in momentum states. These states would disappear if size of the ribbon along the x axis is smaller than $\frac{1}{\Delta k_x}$.

In conclusion, we have studied the electronic structure of gated graphene and graphene ribbons in the Hartree approximation. This permits to include the Coulomb repulsion between the extra carriers and their coupling to the external gate in a selfconsistent manner. We find (eq. (18)) a small departure from the classical linear result $V_G \propto n_{2D}$ which can provide a simple method to measure the slope of the graphene bands. In the case of semiconducting armchair ribbons we have obtained the inhomogeneous distribution of charge carriers q_I and potential U_I along the section of the ribbon. We also find that a finite V_G equal to half their band-gap is necessary to make them conduct.

We acknowledge useful discussions with H. Fertig, P. Jarillo-Herrero, F. Guinea, C. Untiedt, D. Jacob and F. Muñoz-Rojas. This work has been financially supported by MEC-Spain (Grants FIS200402356, MAT2005-07369-C03-01, MAT2006-03471 and the Ramon y Cajal Program), and by Generalitat Valenciana (GV05-152). This work has been partly funded by FEDER funds.

-
- ¹ K. S. Novoselov *et al.*, *Science* **306**, 666 (2004)
 - ² J. Scott-Bunch *et al.* *Nanoletters* **5**, 287 (2005)
 - ³ K. S. Novoselov *et al.*, *Nature* **438**, 197 (2005).
 - ⁴ Y. Zhang *et al.*, *Nature* **438**, 201 (2005).
 - ⁵ C. Berger *et al.*, *Science* **312**, 1191 (2006)
 - ⁶ G. W. Semenoff, *Phys. Rev. Lett.* **54**, 2449 (1984)
 - ⁷ M. I. Katsnelson, *Eur. Phys. J.* **51**, 157 (2006)
 - ⁸ J. Tworzydło, B. Trauzettel, M. Titov, A. Rycerz, C.W.J. Beenakker *Phys. Rev. Lett.* **96**, 246802 (2006)
 - ⁹ S. V. Morozov, K. S. Novoselov, M. I. Katsnelson, F. Schedin, L. A. Ponomarenko, D. Jiang, and A. K. Geim, *Phys. Rev. Lett.* **97**, 016801 (2006)
 - ¹⁰ H. Herschee, P. Jarillo-Herrero, *et. al.*, *Nature* cond-mat/06012121
 - ¹¹ K. Nakada, M. Fujita, G. Dresselhaus and M. S. Dresselhaus, *Phys. Rev. B* **54**, 17954 (1996)
 - ¹² K. Wakabayashi, M. Fujita, H. Ajiki, M. Sigrist, *Phys. Rev. B* **59**, 8271 (1999)
 - ¹³ M. Ezawa, *Phys. Rev. B* **73**, 045432 (2006).
 - ¹⁴ L. Brey and H. Fertig, *Phys. Rev. B* **73**, 235411(2006)
 - ¹⁵ N. M. R. Peres, A. H. Castro Neto, and F. Guinea *Phys. Rev. B* **73**, 195411 (2006). N. M. R. Peres, A. H. Castro Neto, and F. Guinea *Phys. Rev. B* **73**, 239902 (2006)
 - ¹⁶ E. V. Castro *et al.*, cond-mat/0611342
 - ¹⁷ Hongki Min, B.R. Sahu, Sanjay K. Banerjee, A.H. MacDonald, cond-mat/0612236
 - ¹⁸ Young-Woo Son, Marvin L. Cohen, and Steven G. Louie, *Nature* **444**, 347 (2006) Y.-W. Son, M. L. Cohen, and S. G. Louie *Phys. Rev. Lett.* **97**, 216803 (2006)
 - ¹⁹ Zhihong Chen, Yu-Ming Lin, Michael J. Rooks and Phaedon Avouris, cond-mat/0701599.
 - ²⁰ Shahal Ilani, Luke A. K. Donev, Mark Kindermann, and Paul L. McEuen; *Nature Physics*, **2**, 687 (2006)
 - ²¹ *Physical Properties of Carbon Nanotubes*, R Saito, M S Dresselhaus, G Dresselhaus, World Scientific, Singapore (1998)
 - ²² P. K. Park and Sang-Won Kang, *Appl. Phys. Lett.* **89**, 192905 (2006)
 - ²³ F. Muñoz-Rojas *et al.* , *Phys. Rev. B.* **74**, 195417 (2006)
 - ²⁴ P. Jarillo-Herrero , S. Sapmaz, C. Dekker , L.P. Kouwenhoven LP, van der Zant H. *Nature* **429**, 389 (2004)
-